



Regular Article

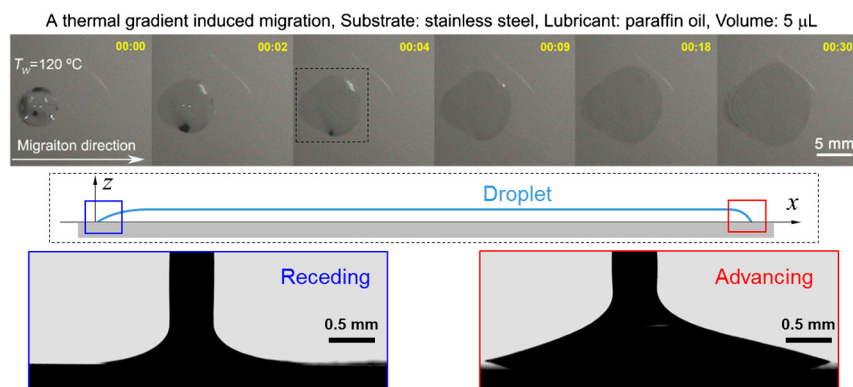
Contact angle hysteresis effect on the thermocapillary migration of liquid droplets

Qingwen Dai*, Wei Huang*, Xiaolei Wang

College of Mechanical and Electrical Engineering, Nanjing University of Aeronautics and Astronautics, Nanjing 210016, China



GRAPHICAL ABSTRACT



ARTICLE INFO

Article history:

Received 17 October 2017

Revised 4 January 2018

Accepted 4 January 2018

Available online 5 January 2018

Keywords:

Thermocapillary migration

Contact angle hysteresis

Interfacial tension

Lubrication approximation

ABSTRACT

Thermocapillary migration describes a phenomenon where a liquid droplet spreads from warm to cold regions due to the interfacial tension gradients. Since the contact angle hysteresis effect is involved during the migration process, we consider the hysteresis effect and rectify the theoretical model to predict the migration velocity on solid surfaces. By conducting migration experiments on surfaces with different magnitudes of the hysteresis effect, we verify the validity of the theoretical derivation. This study advances the understanding of the interfacial phenomenon of thermocapillary migration, moreover, offers an insight into the migration capacity of different materials and guides the design of key components associated with the thermal gradients.

© 2018 Elsevier Inc. All rights reserved.

1. Introduction

The spreading of droplets due to unbalanced interfacial tension forces constitutes an important surface phenomenon, in which chemistry, physics and engineering intersect [1–6]. Typically, the liquid/gas interface tension (γ) is temperature (T) dependent, and

decreases with the increasing of T [7]. When a droplet is placed on a nonuniformly heated solid surface, a tangential force is generated as a consequence of variations in the interfacial tensions, propelling the droplet towards a colder portion [8–11]. This motion is referred to as thermocapillary migration and has attracted considerable attention in tribological systems where thermal gradients are encountered. The thermal flow of lubricants can lead to starvation in contact areas and cause potential lubrication failure [12].

In recent decades, abundant researches have been performed to explore the nature of liquid droplets spreading on a solid surface. It

* Corresponding authors.

E-mail addresses: daiqingwen@nuaa.edu.cn (Q. Dai), huangwei@nuaa.edu.cn (W. Huang).

was originally proposed by Greenspan [13], later specified by Brochard [14] as well as by Ford and Nadim [15], and subsequently validated by several contributions [16–18] that the theoretical model for the thermocapillary migration can be established based on the derivation of the two main forces: the driving force due to the unbalanced interfacial tensions in the vicinity of the three phase contact line and the viscous resistance force. Note that the driving force occurs in the vicinity of the three phase contact line on both sides of a droplet according to Young's equation [19]. It indicates that the driving force is also firmly dependent on the contact angle.

Naturally, most solids are rough and chemically heterogeneous and associate with the pinning of the contact line on surface defects. The wetting and dewetting processes for a liquid droplet on a solid involve the contact angle hysteresis effect [20]. The hysteresis effect impacts the force balance in the vicinity of the three phase contact line on both sides of a droplet [21]. Tadmor et al. [22–24] noted that this effect introduces a lateral retention force acting on the droplet, impeding its motion on a surface. With the introduction of the hysteresis effect, Daniel and Chaudhury [25] rectified the model for the droplet motion induced by vibrations.

Considering the migration procedure, the front edge of a droplet creeps forward, while the rear edge shrinks. In other words, the contact angle of the advancing edge increases while the angle of the receding edge decreases. As a result, a lateral retention force is encountered. This finding means that the driving force originating from the interface tension gradients must overcome this force before the droplet can migrate. A review of the open literature reveals that a theoretical model for taking the hysteresis effect into the thermocapillary migration is currently lacking.

Hence, we theoretically deduce a model to evaluate the migration behavior by including the contact angle hysteresis effect. Since the hysteresis effect varies widely on different material surfaces, four types of materials are employed to characterize the magnitudes of the lateral retention force. Migration experiments of paraffin oil droplets on these surfaces are conducted, and the validity of the theoretical derivation is verified. This study advances the understanding of the interfacial phenomenon of thermocapillary migration, and moreover, via the proposed analytical expressions, migration capacity of different materials can be readily estimated.

2. Materials and methods

A common mineral oil (paraffin oil) is chosen as the tested liquid in all of the experiments. This oil's primary physical parameters are listed in Table 1. The contact angles on different surfaces are measured via the sessile drop method. Firstly, by analyzing the images of a 4 μL sessile drop deposited on a solid surface, the equilibrium contact angle (θ_E) is obtained. Secondly, depositing a drop of approximately 2 μL on a solid with the help of a syringe needle while leaving the tip in the drop, then increasing the drop volume manually while recording images at the same time, the advancing contact angle (θ_A) can be evaluated. In contrast, reducing the drop volume while recording images allows the receding contact angle (θ_R) to be evaluated. All measurements are conducted at the ambient temperature of 20 $^{\circ}\text{C}$ and humidity of 40%.

Table 1
Physical parameters of paraffin oil at 40 $^{\circ}\text{C}$.

Parameter	Values
Kinematic viscosity, m^2/s	5.36×10^{-3}
Density, kg/m^3	889.02
Surface tension gradient coefficient, $\text{N}/(\text{m}^{\circ}\text{C})$	1.295×10^{-4}

The migration experiments are carried out using the apparatus as shown in Fig. 1a. Four different materials (polytetrafluoroethylene (PTFE), stainless steel (SUS 316), aluminum oxide and silicon) are fabricated as the substrates with dimensions of 76 mm \times 30 mm \times 3 mm. The substrate is tightly attached to the temperature controlled elements. Setting the cooling one (T_C) to 0 $^{\circ}\text{C}$ while the heating one (T_W) to 120 or 150 $^{\circ}\text{C}$ generates different thermal gradients on the surface. Fig. 1b shows the accurate temperature distributions obtained by an infrared camera on these four surfaces when $T_C = 0^{\circ}\text{C}$ and $T_W = 120^{\circ}\text{C}$. Obvious differences exist on the thermal gradients because the thermal conductivities of these four materials are different. The measured values of the thermal gradients are all shown in Table 2. Since the temperature on the PTFE surface does not decrease linear along the length of the substrate, the thermal gradient is not shown in this table.

The complete migration process is obtained by a digital video camera. Fig. 1c presents a typical migration phenomenon on a stainless surface. Via extracting the key frames, the droplet height h and migration distance can be measured. In this study, the dosage of paraffin oil for all migration tests is kept constant at 5 μL using a microliter syringe.

3. Results and discussion

3.1. Contact angle hysteresis effect and migration performance

Fig. 2a shows the critical equilibrium (θ_E), advancing (θ_A) and receding (θ_R) contact angles and the calculated values of $(\cos \theta_R - \cos \theta_A)$ on different material surfaces. As shown in the histogram, on the aluminum oxide surface, the values of θ_E , θ_A and θ_R are 8.3 $^{\circ}$, 14.3 $^{\circ}$ and 2.1 $^{\circ}$, respectively, thus θ_E is smaller than θ_R while larger than θ_A . A similar relationship is obtained for the values of θ_E , θ_A and θ_R on the other three material surfaces. It is noted that the corresponding values of θ_E , θ_A and θ_R on these four material surfaces are, in ascending order, aluminum oxide, silicon, stainless steel and PTFE. Moreover, the values of $(\cos \theta_R - \cos \theta_A)$ are calculated and shown in the point line, which are also, in ascending order, aluminum oxide, silicon, stainless steel and PTFE, which is in keeping with the trend of contact angles.

Fig. 2b presents the influence of the materials on the migration velocities induced by the thermal gradients of $T_W = 120^{\circ}\text{C}$ and $T_W = 150^{\circ}\text{C}$. The mean migration velocity of 30 s is chosen as a reference and shown in this figure. The migration experiments are repeated three times, and the relative error of migration velocities is approximately 6%. It can be seen that a higher thermal gradient yields a faster migration velocity. When $T_W = 150^{\circ}\text{C}$, the aluminum oxide surface yields a migration velocity of about 0.5 mm/s, which is 122% higher than the 0.41 mm/s observed for the silicon surface. The migration velocity on the stainless surface is only approximate 0.32 mm/s. The droplet barely moves on the PTFE surface. It is interesting to observe that the trend of migration velocities is opposite to that of $(\cos \theta_R - \cos \theta_A)$ on these four material surfaces which, in descending order, are aluminum oxide, silicon, stainless steel and PTFE.

The experimental results exhibit that the contact angle hysteresis effect plays a significant role in the migration phenomenon, and different migration velocities are obtained on surfaces with different magnitudes of the hysteresis effect. Hence, a theoretical derivation is performed to underlying the mechanism.

3.2. Theoretical hypothesis

For the thermocapillary migration, Brochard [11] and our previous studies [21] noted that the droplet can be regarded as a thin film with curved rim. Referring to Fig. 3, we consider a two

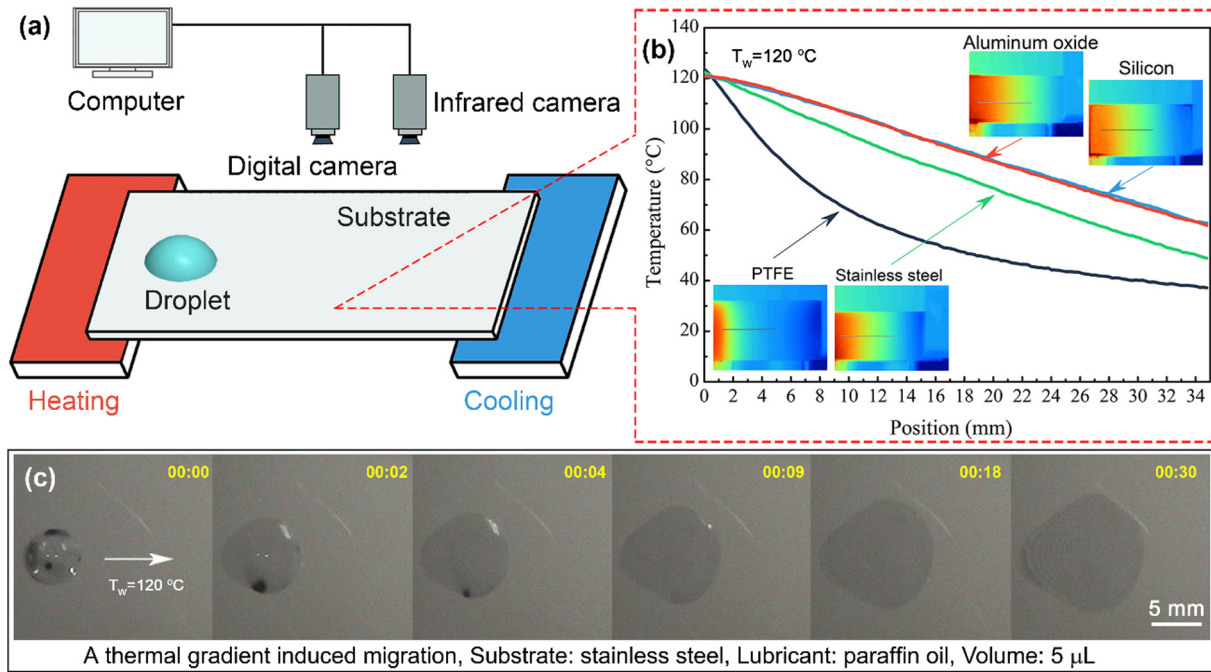


Fig. 1. (a) Schematic diagram of the migration apparatus. (b) Temperature distribution obtained on these four material surfaces when $T_C = 0^\circ\text{C}$ and $T_W = 120^\circ\text{C}$. (c) Typical migration phenomenon on a stainless surface.

Table 2

Measured values of thermal gradients on different material surfaces.

Conditions		Thermal gradient ($^\circ\text{C}/\text{m}$)
$T_C = 0^\circ\text{C}$, $T_W = 120^\circ\text{C}$	Stainless steel	2117
	Silicon	1800
	Aluminum oxide	1800
$T_C = 0^\circ\text{C}$, $T_W = 150^\circ\text{C}$	Stainless steel	2500
	Silicon	2300
	Aluminum oxide	2300

dimensional model of a droplet on an ideal surface exposed to a constant thermal gradient. The contact angle hysteresis effect is presented at the rim, where the advancing contact angle is slightly larger than the receding contact angle. The footprint of the droplet is specified at the positions of X_1 and X_2 in the side view. The h and L are the droplet height and width. The γ , γ_{SL} and γ_{SG} are the liquid/gas, solid/liquid and solid/gas interfacial tensions respectively

(1 refers to X_1 and 2 refers to X_2). The θ_A is the advancing contact angle and θ_R is the receding contact angle.

The quasisteady condition and lubrication approximation theories are always employed for the migration induced by interfacial tension gradients [15,18,26–28]. In this instance, three forces exist on a droplet: the viscous resistance force, the lateral retention force and the unbalanced Young force, which are determined sequentially.

Viscous resistance force. Since the migration progresses slowly in x direction, the z component of the velocity field within the droplet can be ignored. Let V_x denote the x component of the velocity and P denote the pressure. With the thin film lubrication approximation theory applied, the Navier-Stokes and continuity equations decrease to

$$\frac{\partial P}{\partial x} = \mu \frac{\partial^2 V_x}{\partial z^2} \quad (1)$$

where μ is the dynamic viscosity of the liquid.

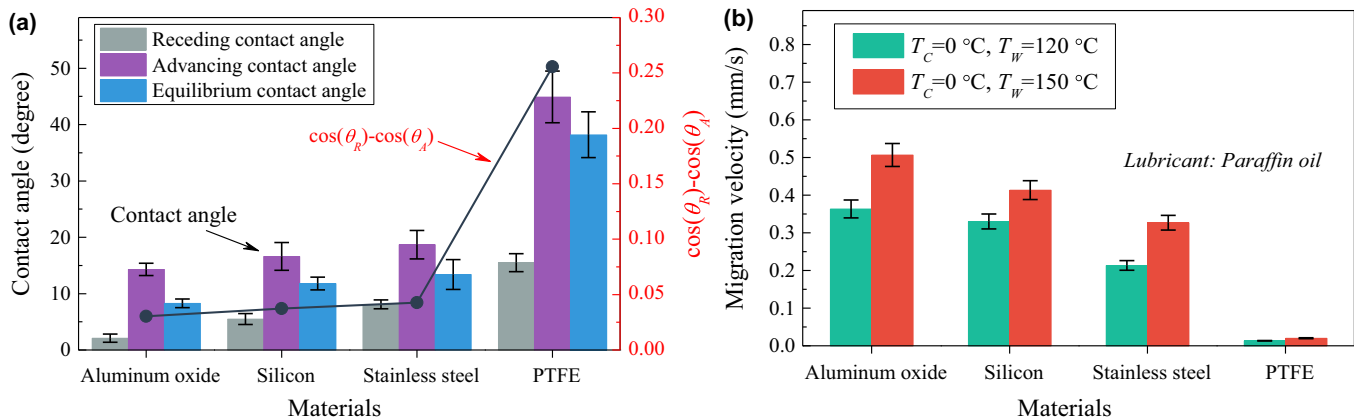


Fig. 2. (a) Critical equilibrium (θ_E), advancing (θ_A) and receding (θ_R) contact angles and the calculated values of $(\cos \theta_R - \cos \theta_A)$ on the different material surfaces. (b) The average migration velocities on these surfaces induced by different thermal gradients of $T_W = 120^\circ\text{C}$ and $T_W = 150^\circ\text{C}$.

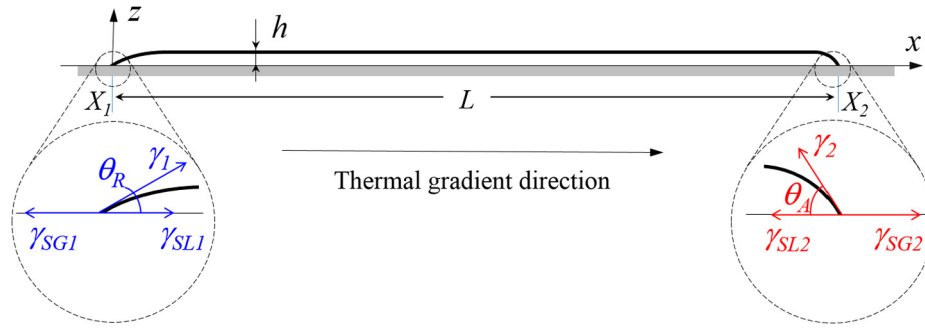


Fig. 3. Droplet on an ideal surface, with the advancing and receding contact angles being shown at the rim.

Assuming a reference coordinate system traveling with the droplet, in this case, the droplet is static while the substrate moves with a velocity of negative U . Therefore, the quasisteady state is reached and the boundary conditions are

$$\begin{cases} \frac{\partial V_x}{\partial z} = \frac{1}{\mu} \frac{\partial \gamma}{\partial x}, z = h(x) \\ V_x = -U, z = 0 \end{cases} \quad (2)$$

The solution for the migration velocity V_x can be derived

$$V_x(z) = \frac{1}{\mu} [C_T \gamma_T z + \frac{1}{2} \cdot \frac{\partial P}{\partial x} (z^2 - 2zh)] - U \quad (3)$$

where C_T denotes the thermal gradient along the x direction on the substrate surface and is obtained via the measured data, and γ_T denotes the surface tension coefficient.

Since the rate of flow across the vertical section of a droplet is zero, we can write

$$\int_0^h V_x(x, y, z) dz = 0 \quad (4)$$

Applying this condition to the velocity distribution equation (Eq. (3)), the viscous stress (σ_{xz}) at the solid/liquid interface satisfying this constraint is given by

$$\sigma_{xz(z=0)} = \mu \left(\frac{\partial V_x}{\partial z} \Big|_{z=0} \right) = \frac{3\mu}{h} U - \frac{1}{2} C_T \gamma_T \quad (5)$$

Note that the constant component of the droplet's height is considerably larger than the varying component (the varying part at the rim). Therefore, h can be treated as constant between the positions X_1 and X_2 , and one arrives at the following equation for the viscous resistance force F_v

$$F_v = \int_{X_1}^{X_2} \sigma_{xz(z=0)} dx = \frac{3\mu}{h} UL - \frac{1}{2} \gamma_T C_T L \quad (6)$$

Lateral retention force. Following the equation derived by Dussan [29] using fluid mechanics considerations and proposed by Tadmor [24,30], the lateral force can be simplified and employed to describe the force acting on the droplet per unit length, $F_{||}$

$$F_{||} = \gamma (\cos \theta_R - \cos \theta_A) \quad (7)$$

Note that lateral retention force $F_{||}$ is also related to the liquid/gas interfacial tension γ . Since the value of γ decreases with increasing temperature, this variation can be described as

$$\gamma_x = \gamma_0 + \frac{\partial \gamma}{\partial x} x = \gamma_0 + C_T \gamma_T x \quad (8)$$

where γ_0 is the surface tension at a reference temperature, and γ_x is the surface tension at the position x , where x scales at the front edge of the droplet.

Unbalanced Young force. The interfacial tension forces balance and contact angle at the triple line was defined by the Young relation [31]

$$\gamma_{SG} = \gamma_{SL} + \gamma \cos \theta_E \quad (9)$$

where θ_E is the equilibrium contact angle.

As shown in Fig. 3, the driving force (F_d) acting on the droplet induced by the unbalanced Young force, is

$$F_d = (\gamma_{SG1} - \gamma_{SL1})_{X_2} - (\gamma_{SG1} - \gamma_{SL1})_{X_1} \quad (10)$$

Combining Eqs. 8–10, the driving force (F_d) can be derived to

$$F_d = \gamma_T C_T L \cos \theta_E \quad (11)$$

Forces balance. The forces acting on the droplet can be deduced from the balance between driving and resistance forces, that is

$$F_d = F_v + F_{||} \quad (12)$$

Substituting Eqs. 6, 7 and 11 into Eq. (12), one finds the following explicit expression for the quasisteady migration velocity U

$$U = \frac{(2 \cos \theta_E + 1) \gamma_T C_T L - 2 \gamma_x (\cos \theta_R - \cos \theta_A)}{6 \mu L} h \quad (13)$$

Moreover, to better describe the experimental situation, three nondimensional parameters of the bond (Bo), capillary (Ca) and Reynold's (Re) numbers are employed and expressed as follows [32]:

$$\begin{aligned} Bo &= \frac{\text{Gravity effects}}{\text{Capillary effects}} = \frac{\rho g R_0^2}{\gamma} \\ Re &= \frac{\text{Inertial effects}}{\text{Viscous effects}} = \frac{\rho U R_0}{\mu} \\ Ca &= \frac{\text{Viscous effects}}{\text{Inertial effects}} = \frac{\mu U}{\gamma} \end{aligned} \quad (14)$$

where R_0 is the planar radius of the droplet.

For the paraffin oil used in this study, the corresponding initial values of these nondimensional parameters under different thermal gradients are calculated and shown in Table 3.

3.3. Theoretical validation

The calculated value of $(\cos \theta_R - \cos \theta_A)$ on the PTFE surface shown in Fig. 2a is significant higher than the value of the other three surfaces. Based on Eq. (13), the initial migration velocity can be calculated, which provides a negative value. This finding means that the driving force cannot overcome the lateral retention force (resistance force) to propel the droplet. The lateral retention force is dominant for droplets on PTFE surfaces, and the slight motion is from the thermal diffusion process. Therefore, in the following sections, migration velocities on the PTFE surfaces are not calculated theoretically. To compare and analyze the experimental

Table 3

Corresponding initial values of these inherent parameters, Bo , Re and Ca , of the droplet under different thermal gradients.

Materials	Thermal gradient ($^{\circ}\text{C}/\text{m}$)	Bo	Re	Ca
Stainless steel	2117	5.49	0.097	0.0045
	2500	5.06	0.1	0.0065
Silicon	1800	4.66	0.11	0.0059
	2300	4.41	0.15	0.011
Aluminum oxide	1800	4.69	0.13	0.0068
	2300	8.28	0.43	0.013

and theoretical results, the immediate migration velocity per second is used.

Fig. 4 shows the typical results of droplet migration on a stainless steel surface induced by a thermal gradient of $T_w = 120^{\circ}\text{C}$. As the scatter diagram shows, the experimental immediate migration velocity is initially rapid, slows gradually, and finally diminishes near zero. The solid line presents the theoretical migration velocities with the consideration of the contact angle hysteresis effect. Note that the predicted values coincide with the experimental data well. When ignoring the hysteresis effect, all of the results are slightly larger in magnitude, as shown by the dotted line. This finding reveals that involving the contact angle hysteresis effect in the theoretical derivation makes the results more reasonable.

To further validate the theoretical description, detailed comparisons between the experimental and theoretical results under different experimental conditions are compared and exhibited in Fig. 5. As the scatter graph in Fig. 5a presents, when $T_w = 120^{\circ}\text{C}$, the initial experimental migration velocity on the stainless steel surface is about 1.6 mm/s, and it decreases quickly as the migration progresses. While for the theoretical velocity, as the line graph presents, it is slightly different with the experimental velocity at first, and in accordance with the experimental data as time elapses. The predicted results of the migration velocities on the silicon and aluminum oxide surfaces coincide with the experimental results well. Nevertheless, a minute difference exists at the beginning, which lasts for approximately 3.5 s.

When $T_w = 150^{\circ}\text{C}$, as shown in Fig. 5b, generally, a higher thermal gradient yields a faster migration velocity. The theoretical predictions are in accordance with the experimental results, both decrease rapidly in the beginning and approach zero gradually. A similar discrepancy exists at the beginning of the trail. As the thermal gradient increases, the initial discrepancy takes approximately 7 s to disappear.

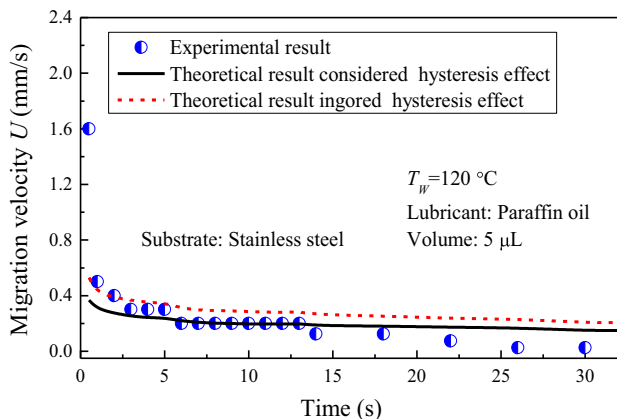


Fig. 4. Typical result of droplet migration on a stainless steel surface induced by a thermal gradient of $T_w = 120^{\circ}\text{C}$.

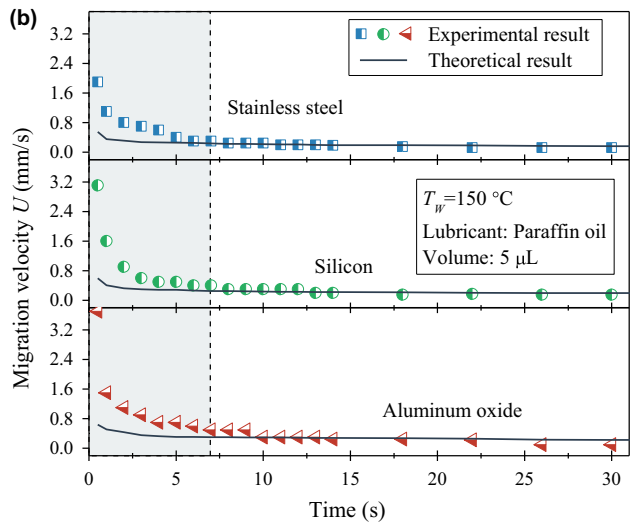
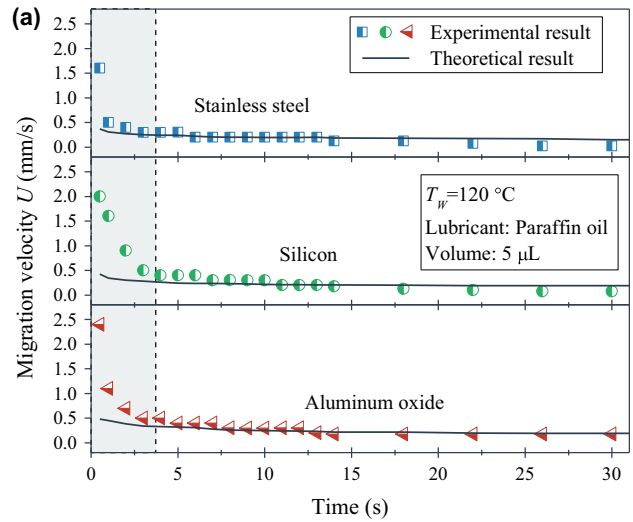


Fig. 5. Comparison between the experimental and theoretical migration results on different material surfaces of stainless steel, silicon and aluminum oxide induced by thermal gradients of (a) $T_w = 120^{\circ}\text{C}$ and (b) $T_w = 150^{\circ}\text{C}$.

3.4. Further discussion

In the present 2D model, we established an appropriate force balance at the advancing and receding edges of the droplet. Three forces act on the droplet: the viscous resistance force, the lateral retention force and the unbalanced Young force. Since the variable component of h at the rim is much lower than the constant component, we substitute a constant h into the derivation of the viscous resistance force. As the migration progresses, the advancing edge of the droplet wets forward, while the receding edge dewets. Therefore, the contact angle hysteresis effect is inevitably involved. Consequently, the lateral retention force always exists at the curved part of the rim, inducing a resistance to the motion. Although Tadmor's recent research [24] proposed the understanding of this lateral retention force, we employ a simplified equation (Eq. (7)) in the theoretical derivation [33,34], which makes the prediction of the migration velocity relatively easy to realize. The theoretical results shown in Fig. 5 conform to the experimental data, however, slight differences exist due to the factors described next.

First, the initial stage of the migration procedure is somewhat complicated. As the droplet ($5\ \mu\text{L}$) placed on the solid surface is subject to a thermal gradient, it spreads to wet the surface rapidly,

which means that the initial velocity is composed of two parts: the wetting velocity and the migration velocity. In the current model, we do not consider the wetting behavior. Moreover, the velocity rapidly increases to its maximum quickly and slows down gradually, indicating that treating the acceleration and deceleration phases as a quasisteady process in the calculation may cause errors. That is the main reason differences exist at the beginning, as the shaded rectangular area shown in Fig. 5. Several numerical studies have demonstrated that the velocities increase markedly from zero to the local maximums within several seconds (<2 s in Ref [35] and <3 s in Ref [36]). A higher initial temperature yields a faster migration velocity, which means that the acceleration phase will be longer. This finding explains why the shaded part in Fig. 5b is larger than that in Fig. 5a (the initial temperature in Fig. 5b is higher).

Second, the advancing and receding contact angles simultaneously decrease with the increasing temperature. This variation is difficult to measure and is not taken into account in the theoretical calculation. Third, there is a small amount of residual oil leaving along its trajectory, and the migration velocity is affected since the droplet volume decreases lightly. A 3D model can be employed for more precise predictions at the expense of additional complications in the derivations and treatment.

The liquid viscosity is also an influencing factor since it decreases with increasing temperature. From the thermography shown in Fig. 1b, the thermal conductivities of these four materials are different, indicating that in reality, the temperatures of droplets on different materials are different. For the thermocapillary migration of a droplet, the surface tension force is the dominant driving force, so the temperature dependence of surface tension is introduced. The paradox is that taking the temperature viscosity effect into consideration will double the error, since the temperature of the droplet is assumed to be the same as the substrate. Ignoring the temperature viscosity effect will also cause the theoretical result to not fit the experimental data well. That issue may also be the original source of the errors.

Generally, the theoretical model presented in this study provides a relatively accurate prediction of the migration velocity based on several assumptions and simplifications. The proposed theoretical derivation is of potential importance in mechanical systems associated with thermal gradients, where liquid lubricants are needed to wet the rubbing surfaces and, alternatively, restrain at the contact area. Measuring the advancing and receding contact angles may help to elucidate the migration capacity of different materials and correspondingly design the key components.

4. Conclusions

By involving the contact angle hysteresis effect, the thermocapillary migration of liquid droplets is investigated experimentally and theoretically in this study. Previous researches [13], [14], [15], [18] revealed that the migration model can be specific by the balance of the interfacial tension force originating from a thermal gradient and viscous resistance force. Relevant studies [22–24], [25] note that the contact angle hysteresis effect brings in a lateral retention force that acts on the droplet impedes the motion while on a surface. Hence, we further hypothesize that the interfacial tension force can be balanced by the viscous resistance and the lateral retention forces. By conducting migration experiments on surfaces with different magnitudes of the hysteresis effect, the validity of the theoretical derivation is verified. This study advances the understanding of the interface phenomenon of droplets migration. More importantly, for mechanical systems encountering thermal gradients, when liquid lubricants are needed to wet the rubbing surface and alternatively, restrain the contact area, the theoretical derivation can offer an insight into the

migration capacity of different materials and provide a guidance to design the key components.

Acknowledgments

The authors are grateful for the financial support provided by the National Natural Science Foundation of China (No. 51675268), the Fundamental Research Funds for the Central Universities (No. NE2017104), and NUAU Research Funding (No: 1005-YAH17045).

References

- [1] M.K. Chaudhury, G.M. Whitesides, How to make water run uphill, *Science* 256 (1992) 1539–1541.
- [2] S. Daniel, M.K. Chaudhury, J.C. Chen, Fast drop movements resulting from the phase change on a gradient surface, *Science* 291 (2001) 633–636.
- [3] R. Tadmor, Marangoni flow revisited, *J. Colloid Interface Sci.* 332 (2009) 451–454.
- [4] E. Bormashenko, Y. Bormashenko, R. Gryniov, H. Aharoni, G. Whyman, B.P. Binks, Self-propulsion of liquid marbles: Leidenfrost-like levitation driven by marangoni flow, *J. Phys. Chem. C* 119 (2015) 9910–9915.
- [5] A. Musin, R. Gryniov, M. Frenkel, E. Bormashenko, Self-propulsion of a metallic superoleophobic micro-boat, *J. Colloid Interface Sci.* 479 (2016) 182–188.
- [6] Q. Lin, Q. Bao, K. Li, M.M. Khonsari, H. Zhao, An investigation into the transient behavior of journal bearing with surface texture based on fluid-structure interaction approach, *Tribol. Int.* 118 (2018) 246–255.
- [7] D. Bonn, J. Eggers, J. Indekeu, J. Meunier, E. Rolley, Wetting and spreading, *Rev. Mod. Phys.* 81 (2009) 739–805.
- [8] P. Bahadur, P.S. Yadav, K. Chaurasia, A. Leh, R. Tadmor, Chasing drops: following escaper and pursuer drop couple system, *J. Colloid Interface Sci.* 332 (2009) 455–460.
- [9] N. Bjelobrk, H.-L. Girard, S. Bengaluru Subramanyam, H.-M. Kwon, D. Quéré, K. K. Varanasi, Thermocapillary motion on lubricant-impregnated surfaces, *Phys. Rev. Fluids* 1 (2016) 063902.
- [10] G. Karapetsas, N.T. Chamakos, A.G. Papanthasiou, Thermocapillary droplet actuation: effect of solid structure and wettability, *Langmuir* 33 (2017) 10838–10850.
- [11] C. Bakli, D.S. P. S. Chakraborty, Mimicking wettability alterations using temperature gradients for water nanodroplets, *Nanoscale* 9 (2017) 12509–12515.
- [12] M. Amiri, M.M. Khonsari, On the thermodynamics of friction and wear—a review, *Entropy* 12 (2010) 1021–1049.
- [13] H.P. Greenspan, On the motion of a small viscous droplet that wets a surface, *J. Fluid Mech.* 84 (1978) 125–143.
- [14] F. Brochard, Motions of droplets on solid surfaces induced by chemical or thermal gradients, *Langmuir* 5 (1989) 432–438.
- [15] M.L. Ford, A. Nadim, Thermocapillary migration of an attached drop on a solid surface, *Phys. Fluids* 6 (1994) 3183–3185.
- [16] P. Ehrhard, S.H. Davis, Non-isothermal spreading of liquid drops on horizontal plates, *J. Fluid Mech.* 229 (1991) 365–388.
- [17] M.K. Chaudhury, A. Chakrabarti, S. Daniel, Generation of motion of drops with interfacial contact, *Langmuir* 31 (2015) 9266–9281.
- [18] V. Pratap, N. Moumen, R.S. Subramanian, Thermocapillary motion of a liquid drop on a horizontal solid surface, *Langmuir* 24 (2008) 5185–5193.
- [19] D.T. Wasan, A.D. Nikolov, H. Brenner, Droplets speeding on surfaces, *Science* 291 (2001) 605–606.
- [20] S. Herminghaus, M. Brinkmann, R. Seemann, Wetting and dewetting of complex surface geometries, *Annu. Rev. Mater. Res.* 38 (2008) 101–121.
- [21] G. Dardelle, P. Erni, Three-phase interactions and interfacial transport phenomena in coacervate/oil/water systems, *Adv. Colloid Interface Sci.* 206 (2014) 79–91.
- [22] R. Tadmor, Line energy, line tension and drop size, *Surf. Sci.* 602 (2008) L108–L111.
- [23] R. Tadmor, P. Bahadur, A. Leh, H.E. N'Guessan, R. Jaini, L. Dang, Measurement of lateral adhesion forces at the interface between a liquid drop and a substrate, *Phys. Rev. Lett.* 103 (2009) 266101.
- [24] R. Tadmor, Approaches in wetting phenomena, *Soft Matter* 7 (2011) 1577–1580.
- [25] S. Daniel, M.K. Chaudhury, Rectified motion of liquid drops on gradient surfaces induced by vibration, *Langmuir* 18 (2002) 3404–3407.
- [26] M.K. Smith, Thermocapillary migration of a two-dimensional liquid droplet on a solid surface, *J. Fluid Mech.* 294 (1995) 209–230.
- [27] R.S. Subramanian, N. Moumen, J.B. McLaughlin, Motion of a drop on a solid surface due to a wettability gradient, *Langmuir* 21 (2005) 11844–11849.
- [28] Q.W. Dai, M.M. Khonsari, C. Shen, W. Huang, X.L. Wang, Thermocapillary migration of liquid droplets induced by a unidirectional thermal gradient, *Langmuir* 32 (2016) 7485–7492.
- [29] E.B. Dussan, On the ability of drops or bubbles to stick to non-horizontal surfaces of solids. Part 2. Small drops or bubbles having contact angles of arbitrary size, *J. Fluid Mech.* 151 (1985) 1–20.

- [30] R. Tadmor, Line energy and the relation between advancing, receding, and young contact angles, *Langmuir* 20 (2004) 7659–7664.
- [31] P. De Gennes, Wetting: statics and dynamics, *Rev. Mod. Phys.* 57 (1985) 827–863.
- [32] E. Kim, J. Baek, Numerical study on the effects of non-dimensional parameters on drop-on-demand droplet formation dynamics and printability range in the up-scaled model, *Phys. Fluids* 24 (2012) 082103.
- [33] E.B. Dussan, R.T.-P. Chow, On the ability of drops or bubbles to stick to non-horizontal surfaces of solids, *J. Fluid Mech.* 137 (1983) 1–29.
- [34] A.I. ElSherbini, A.M. Jacobi, Retention forces and contact angles for critical liquid drops on non-horizontal surfaces, *J. Colloid Interface Sci.* 299 (2006) 841–849.
- [35] H.-B. Nguyen, J.-C. Chen, A numerical study of thermocapillary migration of a small liquid droplet on a horizontal solid surface, *Phys. Fluids* 22 (2010) 062102.
- [36] Z.-B. Wu, Terminal states of thermocapillary migration of a planar droplet at moderate and large marangoni numbers, *Int. J. Heat Mass Transf.* 105 (2017) 704–711.